PCCP

PAPER

View Article Online
View Journal | View Issue

Cite this: *Phys. Chem. Chem. Phys.*, 2023, **25**, 17815

A SIFT-MS study of positive and negative ion chemistry of the *ortho*-, *meta*- and *para*-isomers of cymene, cresol, and ethylphenol†

Stefan J Swift, *[a] Nikola Sixtová, [a] Maroua Omezzine Gnioua [ab] and Patrik Španěl [a]

Received 9th May 2023,
Accepted 19th June 2023

DOI: 10.1039/d3cp02123h

rsc.li/pccp

Selected Ion Flow Tube Mass Spectrometry (SIFT-MS) is a soft ionisation technique based on gas phase ion–molecule reaction kinetics for the quantification of trace amounts of volatile organic compound vapours. One of its previous limitations is difficulty in resolving isomers, although this can now be overcome using different reactivities of several available reagent cations and anions (H_3O^+, NO^+, $O_2^{+\bullet}$, $O^{-\bullet}$, OH^-, $O_2^{-\bullet}$, NO_2^-, NO_3^-). Thus, the ion–molecule reactions of these eight ions with all isomers of the aromatic compounds cymene, cresol and ethylphenol were studied to explore the possibility of their immediate identification and quantification without chromatographic separation. Rate coefficients and product ion branching ratios determined experimentally for the 72 reactions are reported. DFT calculations of their energetics confirmed the feasibility of the suggested reaction pathways. All positive ion reactions proceeded fast but largely did not discriminate between the isomers. The reactivity of the anions was much more varied. In all cases, OH^- reacts by proton transfer forming (M–H); NO_2^- and NO_3^- were unreactive. The differences observed for product ion branching ratios can be used to identify isomers approximately.

1. Introduction

SIFT-MS is a powerful soft mass spectrometric technique that allows for the quantification of volatile organic compounds (VOCs) in the gas-phase, usually air. Whilst analyses of mixtures of multiple analytes are possible, it is currently not easy to analyse isomeric or isobaric species present simultaneously within a matrix. However, as the range of reagent ions available to SIFT-MS has been recently expanded to include anions (H_3O^+, NO^+, $O_2^{+\bullet}$, $O^{-\bullet}$, OH^-, $O_2^{-\bullet}$, NO_2^-, NO_3^-), there is potential to use differing ionic products, produced from the range of reactions to facilitate simultaneous quantification, of isobaric species using SIFT-MS.

Aromatic compounds are an essential chemical class which are analysed in gas-phase complex matrices including human breath;[1–3] headspace of samples such as cosmetics[4] and food stuffs;[5] ambient air for air quality analysis for environmental monitoring purposes;[6–9] as well as investigating ion–molecule reactions, at the centre of the SIFT-MS technique. In particular, aromatic compounds are often of great interest in the field of atmospheric chemistry and air pollution research as many of these species are known to be highly toxic and are released from anthropogenic emissions into the atmosphere, diminishing air quality. Some aromatic compounds may also however be found in human breath[2] and are known to be potential breath biomarkers for certain diseases, such as various cancers,[10] COPD,[11] and polycystic ovarian syndrome.[12]

Previous studies of ion molecule reactions of H_3O^+, NO^+ and $O_2^{+\bullet}$ (in an He carrier gas) have been carried out for several aromatic compounds with *ortho*-, *meta*- and *para*-positioning of chemical groups. This included the three isomers of xylene[13] and the *ortho*- and *para*-isomers of F, Cl, Br and I containing halotoluenes[14] which showed very minor differences in the branching ratios in the $O_2^{+\bullet}$ reaction. Also, work has been conducted[15] which investigated the H_3O^+, NO^+ and $O_2^{+\bullet}$ reactions with *ortho*-, *meta*-, and *para*-cresol, using He carrier gas. Although the separate quantification of the *ortho*-, *meta*-, and *para*-cresol isomers was not possible on the basis of this work when using just the positive reagent ions, recent developments in the SIFT-MS technique has now allowed for the inclusion of negative reagent ions (OH^-, $O_2^{-\bullet}$, $O^{-\bullet}$, NO_2^-, NO_3^-).[16,17] The inclusion of the extra five negative reagent ions means that the classical way of determining the relative reaction rate

[a] *J. Heyrovsky Institute of Physical Chemistry of CAS, v.v.i, Dolejškova 2155/3, 182 23 Prague, Czechia. E-mail: stefan.swift@jh-inst.cas.cz*
[b] *Faculty of Mathematics and Physics, Charles University, Ke Karlovu 3, 120 00 Prague, Czechia*

† Electronic supplementary information (ESI) available. See DOI: https://doi.org/10.1039/d3cp02123h

coefficients (in which all ions are injected at once into the flow tube) is not possible. The inclusion of these negative reagent ion species to SIFT-MS thus warrants further investigation into whether isomers can be identified or even quantified separately within a mixture, based on their differing chemistry with the available reagent ion species.

To survey the potential of the negative ions to differentiate *ortho*-, *meta*- and *para*-isomers, we chose cymene, cresol, and ethylphenol as they are of particular interest in both atmospheric chemistry and disease diagnosis. Cresol is known to be an oxidation product of toluene,[18–20] anthropogenically emitted from vehicle exhaust emissions, for example;[21] the alkylbenzene, cymene, is known to be emitted from municipal solid waste treatment plants[22] and landfill,[22] as well as formed secondarily in the atmosphere;[23] and 4-ethylphenol is known to be found in food stuffs, such as red wine.[24] These compounds have therefore been the basis for our investigation into the ion–molecule reactions occurring when the reagent ions produced by the SIFT-MS instrument interact with these analytes, and how the chemistry changes when functional groups are found in varying positions around the aromatic ring.

The objective of this work was therefore to understand the differences in ion chemistry between the *ortho*-, *meta*-, and *para*-isomers of compounds for the ion–molecule reactions which occur within the flow-tube. Furthermore, to develop on from the previous work we have updated the kinetics library of the ion–molecule reactions, now with negative ions included (as well as within the N_2 carrier gas).

2. Experimental

The principles of SIFT-MS are based on ion–molecule reactions which occur in a flow-tube between reagent ion species and neutral analyte compounds, as to produce varying product ions (even if the species are isobaric or isomeric). The reagent ions are produced in an ion source when a mixture of air and water is presented with microwave radiation from a magnetron to produce a plasma ion soup. The ions in the plasma are attracted towards the first quadrupole and enter the quadrupole mass filter, as to selectively filter one reagent ion to undergo reactions with the neutral analyte species in the flow tube (with either a He or N_2 carrier gas). The product ions are directed through a second quadrupole which is used to analyse the sample matrix. The product ions then hit a detector which sends an electrical signal through to a computer, for which a software package allows for the conversion of this signal to gas-phase concentrations, when the branching ratios and kinetic parameters for a reaction are known.

2.1 Instrument and standards

One of the latest models of the Syft Voice200 series of instruments, the Voice200infinity (Syft Technologies™, New Zealand), was used to analyse 9 aromatic compounds for their branching ratios and rate coefficients when presented with 8 different reagent ion species. In the previous work by Wang *et al.*,[15] a SIFT-MS instrument was used with the three positive reagent ions (H_3O^+, NO^+ and $O_2^{+\bullet}$) to investigate ion–molecule reactions. In recent years however (since 2015),[16] Syft Technologies™ have developed the Voice200infinity instrument which increases the number of possible reagent ions used by this analytical technique, to an extensive 8 reagent ions (with the addition of OH^-, $O_2^{-\bullet}$, $O^{-\bullet}$, NO_2^- and NO_3^-).[16] With a larger number of reagent ions to choose from, a much greater scope of potential ion–molecule reactions is possible and the prospect of measuring *ortho*-, *meta*- and *para*-isomers individually, increases.

To investigate ion–molecule reactions using a SIFT-MS instrument it is preferable to use a container into which analyte standards are injected that doesn't equalise the flow of air and in which the volume of the vessel is able to change easily, without changing the internal pressure. A nalophan sample bag was therefore used in which the bags were filled with dry pure air (generated by zero air generator Parker Hannifin Manufacturing Ltd, Model 636273000) and were spiked separately with the 9 different aromatic compounds, used for SIFT-MS analysis. Nalophan is known to release ethylene glycol,[25] although it is not believed that this would interfere with the aromatic species investigated in this study. Nine different aromatic compounds were analysed, for which a large concentration of standards headspace (from a saturated atmosphere of having injected droplets of standard liquid in to a blank nalophan bag) of each species was injected using a syringe into the nalophan bags, followed by subsequent dilutions. Note that CO_2 produced in the zero air generator was not removed and was thus present in all experiments at a small concentration.

The compounds analysed were *ortho*-cymene, *meta*-cymene and *para*-cymene, *ortho*-cresol, *meta*-cresol, *para*-cresol, *ortho*-ethylphenol, *meta*-ethylphenol and *para*-ethylphenol (all purchased from Sigma-Aldrich as analytical standards). The structures of these compounds are shown in Fig. 1.

A passivated needle (Syft Technologies™) attached to the heated sample injection inlet (cone at 323 K) was pierced into the nalophan bag to sample the gaseous standard compound. Some of the standards were solid at room temperature (*para*-cresol and *para*-ethylphenol) and therefore to keep the species in the gaseous phase, the sampling capillary was heated to 323 K. The analyte molecules then entered a flow of N_2 within the instrument flow tube which was at a temperature of 393 K.

The Voice200infinity is able to produce the required reagent ions from the ion source under three separate conditions required for the positive ion mode (H_3O^+, NO^+ and $O_2^{+\bullet}$), the first negative mode (OH^- and $O_2^{-\bullet}$) as well as the second negative mode ($O^{-\bullet}$, NO_2^- and NO_3^-). After being selected by the quadrupole mass filter, the reagent ions also enter the flow tube and react with the analyte ions. N_2 was the carrier gas used inside the flow tube at a pressure of 410 mTorr. Note that when injecting H_3O^+ into the N_2 carrier gas the relative signals of the reagent ions and their hydrates were 70–80% H_3O^+, 15–30% of $H_3O^+H_2O$ and less than 2% $H_3O^+(H_2O)_2$. Despite the large mass difference between N_2 and He, the branching ratios and rate coefficients for a range of compounds was found not to change

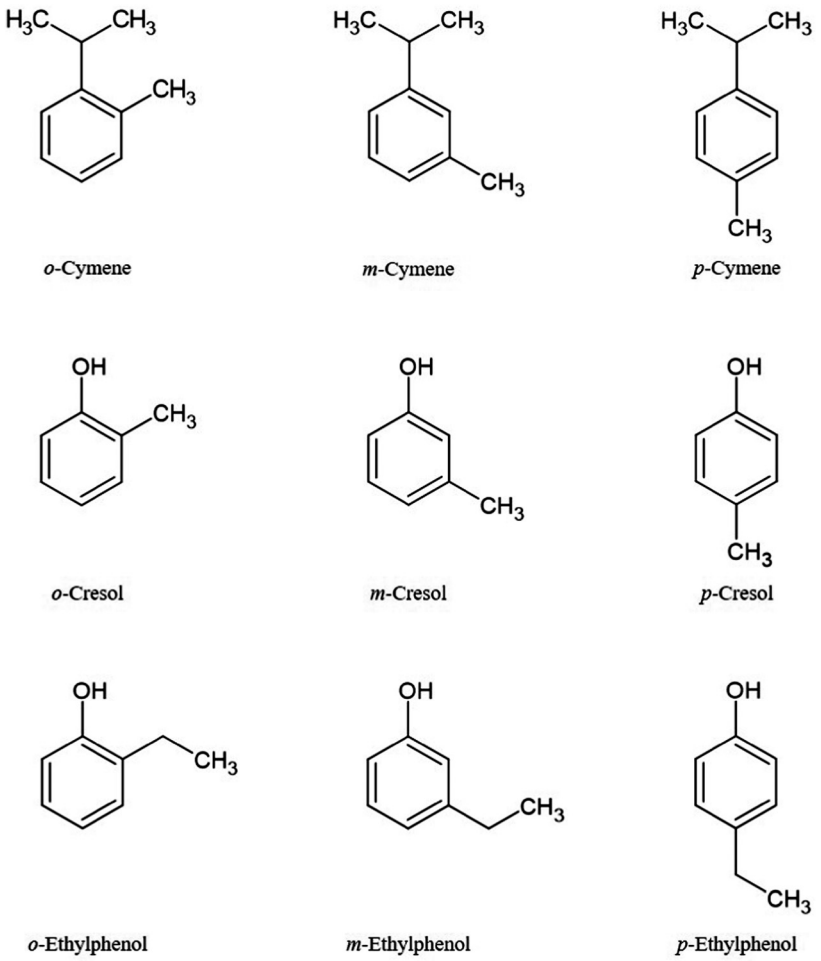

Fig. 1 The structures of the nine compounds investigated in this work.

between these two carrier gases,[26] although the use of N_2 made it necessary to need to dry the instrument out at the start of the day due to the internal condensation of water vapour while the instrument was in standby mode, overnight.

2.2 Determination of product ion branching ratios

The branching ratios were determined by first obtaining full scan spectra in the m/z range 15 to 250, for each reagent ion, for each of the 9 compounds analysed. The major product ions in each of the spectra were identified and an ion list was produced for each compound for the application of the Selected Ion Monitoring (SIM) mode on the Voice200infinity instrument.

The SIM scans were obtained for a nalophan bag filled with zero air (blank), followed by a sequence of different concentrations of neutral analyte species, after injection of the compound headspace into the nalophan bag. The SIM scan mode is able to switch between the three different ion source conditions efficiently. At a constant concentration, 50 measurement data points were obtained for each product ion species across all source conditions (and therefore all reagent ions). This was repeated for several dilutions to obtain data across a range of concentrations.

Only the last 20 data points of each set of product ions were used for data analyses, as the source conditions required time to stabilise the reagent ion concentrations when switching between modes (*N.B.* this is graphically shown in Fig. S1 within the ESI†). The average across these data points was taken and the standard error (SE) was calculated. For each reagent ion, the branching ratios were calculated by summing the total product ion signals and dividing the individual signals by the total product ion count.

In most cases, only one product ion was found, although more complex chemistry was observed with some of the negative reagent ion species. For species which observed more than one reagent ion product, the calculated branching ratios at each concentration were plotted against the count rates of the known major product ions. The intercept of the trend was then taken as the true branching ratio of the reaction.[27]

2.3 Determining reaction rate coefficients

The ion source in the Voice200infinity instrument operates in three separate conditions. These are positive mode; negative mode dry; and negative mode wet. Therefore, it is not possible to inject all the ions simultaneously into the flow tube. As a

result, the relative decay curves cannot be compared to the decay and regeneration of H_3O^+ (known to react *via* proton transfer to the analyte, at the collisional rate coefficient, k_c). To obtain the reaction rate coefficients, the ratio of the total products [P] was divided by the total reagents species (including their hydrates) [R] and the [P]/[R] for each reagent ion, at different stable concentrations (using nalophan bags), for each reaction, were then compared to the reaction of the analyte with H_3O^+ (which occurs at the collisional rate).

The relative slopes of the [P]/[R] were compared to H_3O^+, to give the relative rates of reaction between the reagent ions and the analyte molecule. The relative rates were then multiplied by the k_c of H_3O^+ to calculate the rate coefficient of reaction. The collisional rates were calculated by using the method described by Su and Chesnavich.[28]

2.4 DFT calculations

All quantum chemistry calculations were performed using the ORCA 5.0.1 software. Molecular geometry forms of all neutral *ortho*-, *meta*- and *para*-isomers of aromatic molecules, their protonated forms as well as the product ions resulting from their reaction with the positive and negative reagent ions were first drawn using the AVOGADRO software. These were then further optimised using the ORCA programme with the B3LYP DFT and 6-311++G(d,p) basis set, with a D4 correction. This level of theory was also used to calculate the normal mode vibrational frequencies and thermodynamic quantities of the structures of the neutral molecules and reagent ions. The total enthalpies of all neutral molecules and ions were thus calculated for standard temperature and pressure (298.15 K, 1 atm). The calculations were performed for several feasible structures of each of the ions and the lowest energy structure was then chosen. Enthalpy and entropy changes were then calculated for the neutral and ionic reactants, as well as the products of all reactions. Proton affinities, polarizabilities and dipole moments were also obtained using this DFT method.

3. Results and discussion

The branching ratio and reaction rate kinetics results which are required for the accurate quantification of gas-phase concentrations were carried out under similar conditions in which the Voice200-infinity instrument is routinely used by the majority of its users.

It's known that most of these compounds give only one product ion when using the H_3O^+ and NO^+ ions, although a range of different products were produced when reacting these analyte species in the negative ion mode. The branching ratios calculated for the 9 compounds on their reaction with the available reagent ions in the Voice200infinity are shown in Table 1. As can be seen in Table 1, many reactions resulted in a single product which makes individual calculation simpler, although causes the accurate separate quantification of the three isomeric species for each compound to be more challenging.

The ion products for each reaction were determined by indicating the highest *m*/*z* ion signals and correlating these with the signal at the *m*/*z* value of the known major ion product (based on the reagent ion used) at several different concentrations of the aromatic standard gas. Using the identified product ions for each process, the branching ratios and kinetics were calculated for each species in a N_2 carrier gas, over eight different positive and negative reagent ions. The results for these reaction rate coefficients are shown in Table 2.

3.1 Positive ions

The three available positive ions, H_3O^+, NO^+ and $O_2^{+\bullet}$ are the basis of most of the ion–molecule reactions using SIFT-MS known to date, up until 2015.[16] Four of the aromatic compounds presented in this study (*ortho*-, *meta*- and *para*-cresol as well as *para*-ethylphenol) have earlier been investigated using He carrier gas at 300 K in previous work[15] when negative ions were not available for SIFT-MS studies. We therefore extend the knowledge of ion–molecule reactions with positive reagent ions, by elaborating the library for the other aromatic species presented in this study.

In comparison to the previous work conducted in He for the cresol isomers as well as 4-ethylphenol (Table 2), the collisional rate coefficients (k_c) are slightly lower for the work in N_2 with a flow tube temperature of 393 K. This is predominantly due to the increase in carrier gas temperature. The present experimental rate coefficients are also similar to the previous work in He (296–300 K).[15] This agrees with the findings of our previous comparison study, which showed that rate coefficients conducted in He and N_2 carrier gases (using a *Profile* 3 instrument) do not significantly change with carrier gas.[26] The previous *k* values are generally slightly higher (see Table 2) which is most likely down to the increased flow tube temperature of the Voice200infinity.

3.1.1 H_3O^+ reactions. H_3O^+ reactions occur at the collisional rate, when the proton affinity for the analyte is greater compared to that of water (>691 kJ mol^{-1}).[30] This is seen for all nine compounds included in this study. No ligand switching reaction of the $H_3O^+{\cdot}H_2O$ hydrate was observed in addition to proton transfer.

Note that for cymene, a minor fragment product ion is formed at *m*/*z* 93, alongside the major proton transfer product.

$$H_3O^+ + C_{10}H_{14} \rightarrow C_{10}H_{15}^+ + H_2O \quad (1a)$$

$$\rightarrow C_7H_9^+ + C_3H_7OH \quad (1b)$$

The DFT calculations showed that the proton transfer (reaction (1a)) was exothermic by 30 kJ mol^{-1}, 22 kJ mol^{-1} and 44 kJ mol^{-1} for the *ortho*-, *meta*- and *para*-isomers, respectively, but that dissociative proton transfer forming separate C_3H_6 and H_2O products would be endothermic by 13 to 19 kJ mol^{-1}. This means that the dissociative channel corresponding to the ion product at *m*/*z* 93 ($C_7H_9^+$) must proceed as indicated in reaction (1b), forming a propanol neutral product. The calculated enthalpy changes confirm this idea, as they are -19 kJ mol^{-1} (*ortho*-), -13 kJ mol^{-1} (*meta*-) and -13 kJ mol^{-1} (*para*-), for 1-propanol and -36 kJ mol^{-1} (*ortho*-), -30 kJ mol^{-1} (*meta*-) and -30 kJ mol^{-1} (*para*-) for 2-propanol. Note that another possible

Table 1 Product ion branching ratios determined for the reactions between the 9 aromatic compounds investigated in this study from the reaction with the 8 separate possible reagent ions which may be produced by the Voice200infinity instrument, for reactions which take place in a N_2 carrier gas only. For each product ion the *m/z* is given before the molecular formula and the branching ratio is shown in parentheses

Compound		H_3O^+	NO^+	$O_2^{+\bullet}$	$O^{-\bullet}$	OH^-	$O_2^{-\bullet}$	NO_2^-	NO_3^-
Cymene	*ortho-*	135 $C_{10}H_{15}^+$ (94) 93 $C_7H_9^+$ (6)	134 $C_{10}H_{14}^{+\bullet}$ (100)	134 $C_{10}H_{14}^{+\bullet}$ (10) 119 $C_9H_{11}^+$ (90)	—[a]	133 $C_{10}H_{13}^-$ (88) 119 $C_8H_7O^-$ (12)	—	—	—
	meta-	135 $C_{10}H_{15}^+$ (98) 93 $C_7H_9^+$ (2)	134 $C_{10}H_{14}^{+\bullet}$ (100)	134 $C_{10}H_{14}^{+\bullet}$ (23) 119 $C_9H_{11}^+$ (77)	—	133 $C_{10}H_{13}^-$ (99) 119 $C_8H_7O^-$ (1)	—	—	—
	para-	135 $C_{10}H_{15}^+$ (96) 93 $C_7H_9^+$ (4)	134 $C_{10}H_{14}^{+\bullet}$ (100)	134 $C_{10}H_{14}^{+\bullet}$ (10) 119 $C_9H_{11}^+$ (90)	—	133 $C_{10}H_{13}^-$ (97) 119 $C_8H_7O^-$ (3)	—	—	—
Cresol	*ortho-*	109 $C_7H_8OH^+$ (100)	108 $C_7H_8O^{+\bullet}$ (100)	108 $C_7H_8O^{+\bullet}$ (98) 107 $C_7H_7O^+$ (2)	109 $C_6H_5O_2^-$ (2) 107 $C_7H_7O^-$ (83) 106 $C_7H_6O^{-\bullet}$ (15)	107 $C_7H_7O^-$ (100)	140 $C_7H_8O{\cdot}O_2^{-\bullet}$ (16) 107 $C_7H_7O^-$ (84)	154 $C_7H_8O{\cdot}NO_2^-$ (100)	170 $C_7H_8O{\cdot}NO_3^-$ (100)
	meta-	109 $C_7H_8OH^+$ (100)	108 $C_7H_8O^{+\bullet}$ (100)	108 $C_7H_8O^{+\bullet}$ (99) 107 $C_7H_7O^+$ (1)	109 $C_6H_5O_2^-$ (2) 107 $C_7H_7O^-$ (92) 106 $C_7H_6O^{-\bullet}$ (6)	107 $C_7H_7O^-$ (95) 93 $C_6H_5O^-$ (5)	140 $C_7H_8O{\cdot}O_2^{-\bullet}$ (29) 107 $C_7H_7O^-$ (71)	154 $C_7H_8O{\cdot}NO_2^-$ (100)	170 $C_7H_8O{\cdot}NO_3^-$ (100)
	para-	109 $C_7H_8OH^+$ (100)	108 $C_7H_8O^{+\bullet}$ (100)	108 $C_7H_8O^{+\bullet}$ (98) 107 $C_7H_7O^+$ (2)	109 $C_6H_5O_2^-$ (1) 107 $C_7H_7O^-$ (83) 106 $C_7H_6O^{-\bullet}$ (16)	107 $C_7H_7O^-$ (97) 93 $C_6H_5O^-$ (3)	140 $C_7H_8O{\cdot}O_2^{-\bullet}$ (39) 107 $C_7H_7O^-$ (61)	154 $C_7H_8O{\cdot}NO_2^-$ (100)	170 $C_7H_8O{\cdot}NO_3^-$ (100)
Ethylphenol	*ortho-*	123 $C_8H_{10}OH^+$ (100)	122 $C_8H_{10}O^{+\bullet}$ (100)	122 $C_8H_{10}O^{+\bullet}$ (33) 107 $C_7H_7O^+$ (67)	121 $C_8H_9O^-$ (95) 119 $C_8H_7O^-$ (5)	121 $C_8H_9O^-$ (100)	154 $C_8H_{10}O{\cdot}O_2^{-\bullet}$ (25) 121 $C_8H_9O^-$ (75)	168 $C_8H_{10}O{\cdot}NO_2^-$ (100)	—
	meta-	123 $C_8H_{10}OH^+$ (100)	122 $C_8H_{10}O^{+\bullet}$ (100)	122 $C_8H_{10}O^{+\bullet}$ (76) 107 $C_7H_7O^+$ (24)	121 $C_8H_9O^-$ (97) 119 $C_8H_7O^-$ (3)	121 $C_8H_9O^-$ (100)	154 $C_8H_{10}O{\cdot}O_2^{-\bullet}$ (48) 121 $C_8H_9O^-$ (52)	168 $C_8H_{10}O{\cdot}NO_2^-$ (100)	—
	para-	123 $C_8H_{10}OH^+$ (100)	122 $C_8H_{10}O^{+\bullet}$ (100)	122 $C_8H_{10}O^{+\bullet}$ (35) 107 $C_7H_7O^+$ (65)	121 $C_8H_9O^-$ (89) 119 $C_8H_7O^-$ (11)	121 $C_8H_9O^-$ (100)	154 $C_8H_{10}O{\cdot}O_2^{-\bullet}$ (55) 121 $C_8H_9O^-$ (45)	168 $C_8H_{10}O{\cdot}NO_2^-$ (100)	—

[a] — Indicates no reaction.

Table 2 List of aromatic compounds investigated in this work with their associated molecular parameters as well as their experimentally determined rate coefficients (k, $\times 10^{-9}$ cm^3 s^{-1}) and their theoretically calculated collisional rate coefficients [k_c, $\times 10^{-9}$ cm^3 s^{-1}] (given in square brackets) for their reactions with each of the 8 possible reagent ions which may be produced by the Voice200infinity instrument, for reactions which take place in a N_2 carrier gas only. The values in bold represent previous data collected using a He carrier gas and a carrier gas temperature of room temperature (296–300 K)[15]

Compound		PA (kJ mol^{-1})	I.E. (eV)	Polarizability α, Å^3 ($\times 10^{-24}$ cm^3)	Dipole moment D, Debye	H_3O^+ [k_c]	NO^+ k [k_c]	O_2^+• k [k_c]	O^- k [k_c]	OH^- k [k_c]	O_2^-• k [k_c]	NO_2^- k [k_c]	NO_3^- k [k_c]
Cymene	*ortho-*	717		17.4	0.68	[2.6]	2.2 [2.1]	2.0 [2.1]	—[b]	0.3 [2.7]	—	—	—
	meta-	710		17.6	0.34	[2.5]	2.2 [2.0]	2.0 [2.0]	—	0.1 [2.6]	—	—	—
	para-	731	8.29[a]	17.7	0.06	[2.4]	2.2 [2.0]	2.0 [2.0]	—	0.1 [2.6]	—	—	—
Cresol	*ortho-*	752	8.46[a]	12.6	1.06	[2.4], **[2.8]**	2.2 [2.0], **2.2 [2.3]**	1.8 [2.0], **2.2 [2.3]**	0.3 [2.6]	1.1 [2.5]	0.9 [2.0]	0.1 [1.7]	0.0 [1.5]
	meta-	754	8.29[a]	12.7	1.07	[2.4], **[2.8]**	2.1 [2.0], **2.0 [2.3]**	1.8 [2.0], **2.1 [2.3]**	0.2 [2.6]	0.9 [2.5]	0.8 [2.0]	0.1 [1.7]	0.0 [1.6]
	para-	759	8.34[a]	12.7	1.46	[2.6], **[2.8]**	2.3 [2.2], **2.2 [2.3]**	2.0 [2.1], **2.2 [2.3]**	0.3 [2.8]	1.0 [2.8]	0.8 [2.1]	0.1 [1.9]	0.0 [1.7]
Ethylphenol	*ortho-*	756		14.5	1.11	[2.6]	2.1 [2.1]	1.9 [2.1]	0.3 [2.8]	1.0 [2.7]	0.9 [2.1]	0.2 [1.8]	—
	meta-	756		14.5	1.07	[2.5]	2.3 [2.1]	2.0 [2.0]	0.3 [2.7]	0.9 [2.7]	0.9 [2.0]	0.2 [1.8]	—
	para-	758	7.84[a]	14.6	1.44	[2.7], **[2.8]**	2.6 [2.3], **2.4 [2.3]**	2.5 [2.2], **2.4 [2.2]**	0.3 [2.9]	1.2 [2.9]	1.1 [2.2]	0.2 [1.9]	—

All the PA, α and D values have been calculated from theoretical DFT calculations using the B3LYP DFT and the basis set 6-311++G(d,p) with the D4 correction. [a] Taken from the NIST database.[29] [b] — Indicates no reaction.

ion product at m/z 93 could be $C_6H_5O^+$, although it's formation would be endothermic (with butane and H_2 as the neutral products) by more than 158 kJ mol^{-1} for all isomers, and would also require a substantial amount of rearrangement to produce, from a cyclic aromatic species.

The production of a small amount of $C_7H_9^+$ from cymene is caused by the loss of the C_3H_6 group from the main benzene π-system. Alkyl groups are known to be electron donating and are more so, the larger the carbon chain. The electron donating group enriches the π-system and makes the molecule more susceptible to electrophilic attack by the H_3O^+ ion, resulting in formation of a fragment at m/z 93 ($C_7H_9^+$). Table 1 also shows that the branching ratios are different between the different isomers of cymene, for m/z 135 ($C_{10}H_{15}^+$) and m/z 93 ($C_7H_9^+$). Although m/z 93 is a minor product ion, the difference in branching ratios indicates some possibility for identification of these species from the H_3O^+ SIFT-MS data. Table 1 shows that the *ortho-* (6%) isomer produces the greatest fraction of $C_7H_9^+$, followed by the *para-* (4%) and *meta-* (2%) species. The difference in branching ratios may be somewhat influenced by the different exothermicities of reaction (1b) for the different isomers due to the relative positioning of the methyl group with respect to the isopropyl group.

Electron donating groups are known to cause the next additional substituent to add to the *para-* or *ortho*-positions of benzene rings. This is because there is a greater stabilisation of the cation, when the positive charge is located on the carbon (in the benzene ring) which is attached directly to the isopropyl group (as the isopropyl group is electron donating). When H^+ adds to the *ortho-* or *para*-position of the cymene (with respect to the isopropyl group), this causes a resonance structure where the positive charge is able to spend some time on the carbon which is directly attached to the isopropyl group. This therefore makes the H^+ addition to either the *ortho-* or *para*-position of the aromatic (with respect to the isopropyl group) more favourable (Fig. 2).

When the H^+ adds to the aromatic species, having the CH_3 group in the *meta*-position with respect to the isopropyl group means that the delocalised positive charge does not dwell on the aromatic carbon directly attached to the isopropyl group. There is therefore a higher transition energy associated with this mechanism resulting in the lowest branching ratio (m/z 93, 2%) being associated with the *meta*-cymene species.

The *ortho*-cymene isomer produces the highest fraction of the $C_7H_9^+$ fragment, which is most likely due to the isopropyl and methyl groups being adjacent to one another. This would cause a greater electron density to persist between carbons 1 and 2 on the benzene ring. The greater fraction of electron density would allow for better stability for the cation intermediate when the positive charge is located on carbon 1 and therefore the loss of the isopropyl cation is more susceptible in the *ortho*-cymene species.

However, no fragmentation was seen for any of the cresol or ethylphenol isomers.

$$H_3O^+ + C_7H_8O \rightarrow C_7H_8OH^+ + H_2O \quad (2)$$

$$H_3O^+ + C_8H_{10}O \rightarrow C_8H_{10}OH^+ + H_2O \quad (3)$$

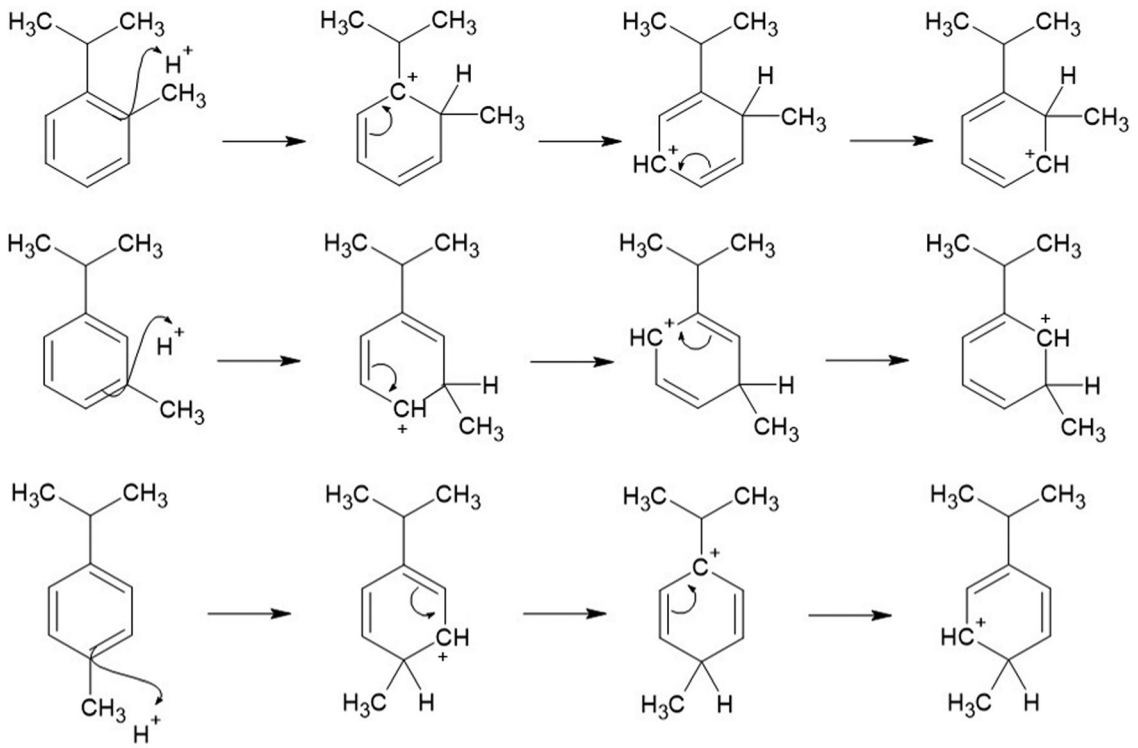

Fig. 2 Resonance stabilisation structures of the cation intermediates of the *ortho*- (top) *para*- (middle) and *meta*- (bottom) cymene species.

Note that cresol (reaction (2)) and ethylphenol (reaction (3)) have shorter alkyl groups as well as an electron withdrawing (–I) OH group attached to the benzene ring, which reduces the richness of the π-system on the benzene ring and therefore causes less of an attraction for the H_3O^+ electrophile.

3.1.2 NO^+ reactions. In the reaction of each species with NO^+ for each isomer, the reaction always takes the charge transfer pathway to produce the radical molecular cation (in agreement with Wang *et al.*[15]).

$$NO^+ + C_{10}H_{14} \rightarrow C_{10}H_{14}{}^{+\bullet} + NO^\bullet \quad (4)$$

$$NO^+ + C_7H_8O \rightarrow C_7H_8O^{+\bullet} + NO^\bullet \quad (5)$$

$$NO^+ + C_8H_{10}O \rightarrow C_8H_{10}O^{+\bullet} + NO^\bullet \quad (6)$$

This is because the ionisation energies of all nine molecules are below that of $NO^\bullet$ (9.26 eV).[29] As there is no differentiation here between these product ions and as the rate coefficients (Table 2) are very similar between isomers, the reactions involving NO^+ are less useful for identification purposes.

3.1.3 $O_2^{+\bullet}$ reactions. $O_2^{+\bullet}$ reactions with VOCs often proceed *via* charge transfer forming a radical molecular cation. Analogous to electron ionisation, this can result in fragmentation which somewhat limits the value of using $O_2^{+\bullet}$ as the reagent ion of choice in the SIFT-MS analysis of mixtures of analytes. Nevertheless, differences in fragmentation patterns are sometimes useful for isomer identification. All 9 compounds show the charge transfer product with one additional fragment. This indicates the relative softness of $O_2^{+\bullet}$ ionisation of these particular aromatic species. This may be due to the generally larger size of aromatic species investigated here (compared to smaller VOCs) and therefore the energy released in charge transfer can distribute over a large number of degrees of freedom.

3.1.3.1 Cymene. The two product ions formed from the interaction of $O_2^{+\bullet}$ with cymene are the molecular radical cation $C_{10}H_{14}{}^{+\bullet}$ (*m*/*z* 134) and a fragment ion formed after the loss of a $CH_3^\bullet$ ($C_9H_{11}^+$, *m*/*z* 119), formed by the reactions:

$$O_2^{+\bullet} + C_{10}H_{14} \rightarrow C_{10}H_{14}{}^{+\bullet} + O_2 \quad (7a)$$

$$\rightarrow C_9H_{11}{}^+ + CH_3^\bullet + O_2 \quad (7b)$$

For all isomers, the main product ion is the fragment $C_9H_{11}{}^+$ (*m*/*z* 119) which results from the loss of a methyl group (it is however not entirely clear which $CH_3^\bullet$ group is lost). Note that the *meta*-isomer reaction leaves the highest fraction of the radical cation $C_{10}H_{14}{}^{+\bullet}$ (*m*/*z* 134, 23%) and that the available EI spectra do not indicate any significant differences in the *m*/*z* 134 fraction between the three isomers (all being about 20%).

The relative branching ratios for the separate isomers may however potentially be explained by resonance stabilisation of the transition intermediate. In the *ortho*- and *para*-isomers, the positive charge is able to become stabilised by the +I effect of the isopropyl group (assuming the methyl group is lost) which gives this transition state a lower relative enthalpy of formation, compared to that of the *meta*-isomer. This therefore explains the lower branching ratio of the $C_9H_{11}{}^+$ (*m*/*z* 109) fragment ion product for the *meta*-isomer compared to the *ortho*- or *para*-isomers (Table 1).

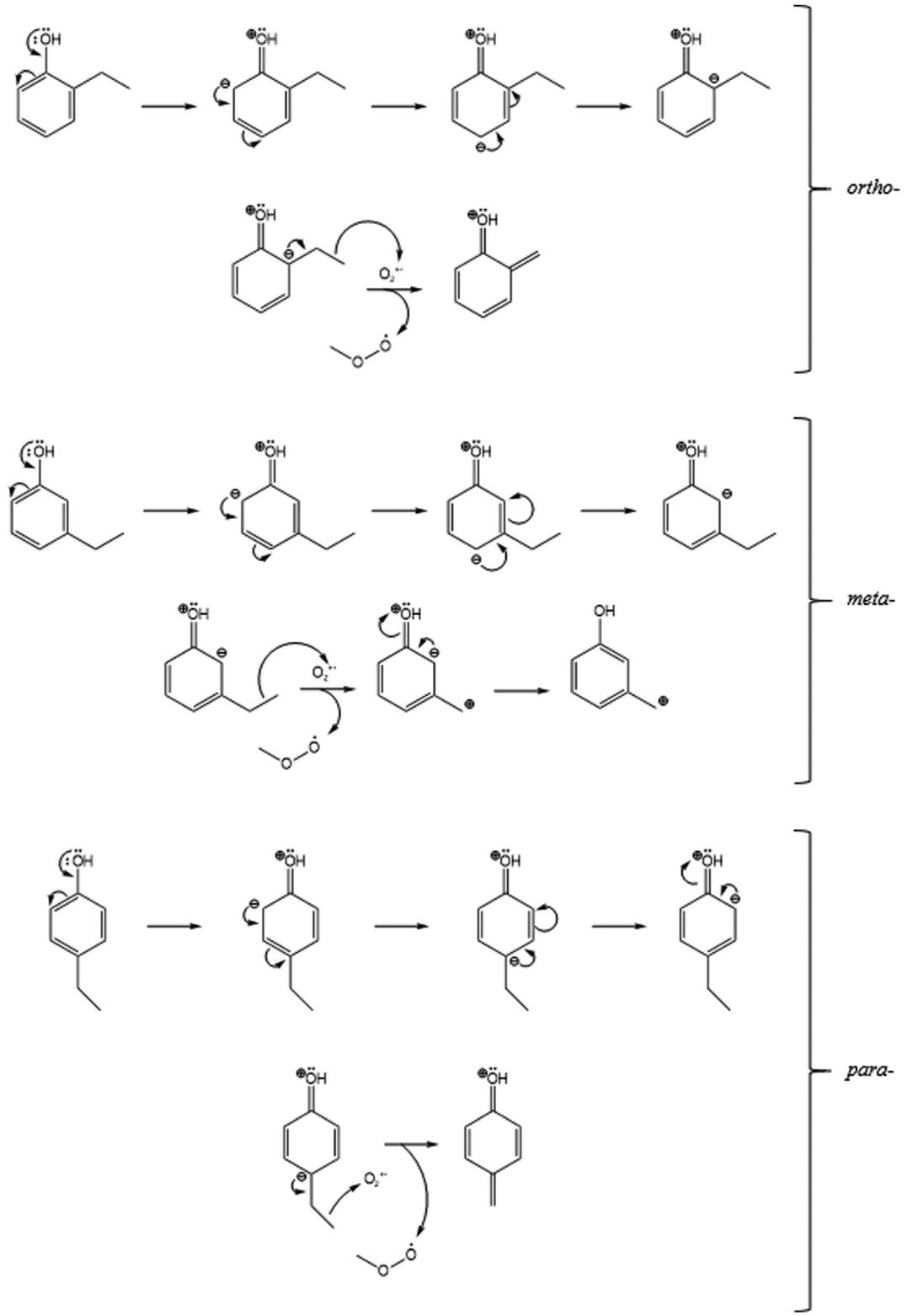

Fig. 3 The mesomeric effect and the resonance structures of the *ortho*- (top) and *meta*- (middle) and *para*- (bottom) isomers of ethylphenol (for reaction (9b)), followed by reaction with the $O_2^{+\bullet}$ reagent ion.

3.1.3.2 Cresol. The $O_2^{+\bullet}$ reactions with all three cresol isomers predominantly produce a single charge transfer product (agreeing with the previous work in He);[15]

$$O_2^{+\bullet} + C_7H_8O \rightarrow C_7H_8O^{+\bullet} + O_2 \quad (8a)$$

$$\rightarrow C_7H_7O^+ + H^\bullet + O_2 \quad (8b)$$

Electron Ionisation spectra (from the NIST database)[29] show that the *para*-isomer of cresol fragments mostly into *m*/*z* 107 (47%) and *m*/*z* 77 (14%), as well as leaving the unfragmented molecular cation (*m*/*z* 108, 40%). The full scans of cresol from the Voice200infinity however only show a small percentage of the *m*/*z* 107 ion product. This is surprising based on the high energetics of the $O_2^{+\bullet}$ reagent, although this does agree with the previous literature.[15]

3.1.3.3 Ethylphenol. The main product ions were the radical cation $C_8H_{10}O^{+\bullet}$ and the fragment ion, $C_7H_7O^+$ (*m*/*z* 107):

$$O_2^{+\bullet} + C_8H_{10}O \rightarrow C_8H_{10}O^{+\bullet} + O_2 \quad (9a)$$

$$\rightarrow C_7H_7O^+ + CH_3^\bullet + O_2 \quad (9b)$$

However, the molecular ion is the main product only for the *meta*-isomer whilst it is a minor product of the *ortho*- and *para*-isomers. Note that the *m*/*z* 107 fragment ion is the base peak on the EI spectra.[29] It is surprising that $O_2^{+\bullet}$ produces very few fragments (reaction (9a) and (9b)) with ethylphenol as it is known that $O_2^{+\bullet}$ is a radical and that organic radical cations tend to split species up into fragments.

This is however confirmed by the previous work in He.[15] Analogues to cymene, the percentage of the unfragmented charge transfer product is seen to be largest in the *meta*-isomer (a trend similar to the EI spectra).

This may be explained by a +M mesomeric effect which is induced by the OH group in ethylphenol. The OH group causes the shown resonance structures within the three isomers of ethylphenol (Fig. 3).

These resonance forms show that the negative charge may dwell on both the *ortho*- and *para*-carbons, relative to the OH group (Fig. 3). As a result, the negative charge may be more stable around the ethyl groups in the *ortho*- and *para*-positions, making these intermediates more prone to attack by the positive $O_2^{+\bullet}$ ion. This may be the reason for the higher $C_7H_7O^+$ (*m*/*z* 107) in the *ortho*- and *para*-isomers.

Furthermore (and very similar to the NO^+ reactions) little difference is seen between the relative rates of the isomeric species of each compound, although for both cresol and ethylphenol, the fastest reaction occurs when the methyl group is located in the *para*-position, which is most likely due to a reduction in sterical hindrance here.

3.2 Negative ions

The negative ion reactions with the aromatic compounds included in this study have not been studied (to the best of our knowledge) to date. In order to extend the number of possible ways to measure these aromatic isomers, it is necessary to extend the number of possible ion–molecule reaction pathways and therefore the differing ion products, rates and branching ratios which label a process. In this work, we therefore report the reaction rate coefficients and branching ratios and describe the chemistry occurring within the flow tube for the nine compounds with the negative reagent ions available in the Voice200infinity SIFT-MS instrument. DFT calculations of the enthalpy changes were carried out to support the proposed reaction pathways.

Overall, it is seen that the negative ions have a significantly slower reaction compared to the positive ions (see Table 2). This is most likely due to the over-crowding of the negative π-system which hinders the negative ion chemistry. In addition, it is seen that these negative reagent ion–molecule reaction processes only produce either one or two ion products (including adducts).

3.2.1 $O^{-\bullet}$ reactions

3.2.1.1 Cymene. The rate coefficients $O^{-\bullet}$ reactions with all three isomers was immeasurably slow ($<10^{-11}$ cm^3 s^{-1}) and therefore they are not given in Table 2. Nevertheless, very low count rates of the $C_{10}H_{13}^-$ product ion were detected:

$$O^{-\bullet} + C_{10}H_{14} \rightarrow C_{10}H_{13}^- + OH^\bullet \quad (10)$$

We conducted DFT calculations to test where exactly the most likely position would be, where a proton would be transferred from. In the case of the *ortho*-cymene structure it was found that removing H^+ from the benzene ring or the isopropyl group would be endothermic, so H^+ must originate from the methyl group, when the reaction is exothermic by 13 kJ mol^{-1}. This therefore indicates that this reaction is energetically possible as a proton transfer to $O^{-\bullet}$ from the methyl group (directly attached to the benzene ring) in cymene. The low exothermicity may also explain why the reaction (10) is very slow.

3.2.1.2 Cresol. The reactions of $O^{-\bullet}$ with C_7H_8O show the production of three product ion species. The product ions were identified as:

$$O^{-\bullet} + C_7H_8O \rightarrow C_6H_5O_2^- + CH_3^\bullet \quad (11a)$$

$$\rightarrow C_7H_7O^- + OH^\bullet \quad (11b)$$

$$\rightarrow C_7H_6O^{-\bullet} + H_2O \quad (11c)$$

The major product in the $O^{-\bullet}$ reactions with all three isomers is $C_7H_7O^-$, produced *via* reaction (11b). Table 1 shows that the highest proportion of this product is produced by the *meta*-isomer (92%, $\Delta H = -142$ kJ mol^{-1}), followed by *ortho*-isomer (83%, $\Delta H = -146$ kJ mol^{-1}) and *para*-isomer (83%, $\Delta H = -140$ kJ mol^{-1}). The *meta*-isomer exhibits the highest proportion of the $C_7H_7O^-$ product most likely because the $O^{-\bullet}$ reagent ion abstracts a hydrogen from the phenolic OH group (which has the greatest δ^+ charge). This would produce the following resonance structures (Fig. 4).

In doing so, this would produce a resonance structure in which the negative charge does not dwell on the *meta*-carbon at any point. As a result, the +I effect from the methyl group does not repel against the negative charge (whereas for the *ortho*- and *para*-isomers this does happen). Correspondingly, this causes the *meta*-cresol transition state to be the most energetically favourable and therefore explains why the *meta*-cresol isomer produces the largest fraction of the proton transfer product ($C_7H_7O^-$).

The second most abundant product is $C_7H_6O^{-\bullet}$ (reaction (11c)), in which H_2O is produced as a neutral product. The ΔH values for

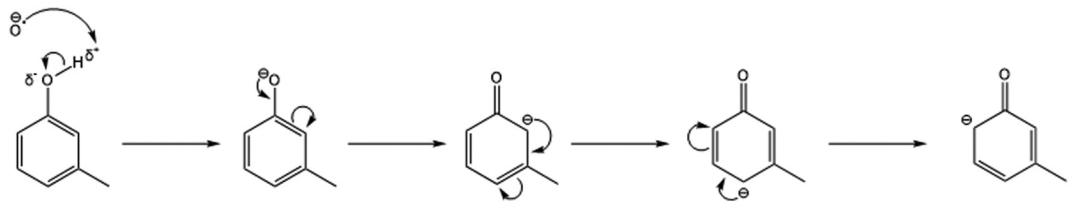

Fig. 4 Resonance stabilisation structures of the reaction anion intermediate when the $O^{-\bullet}$ nucleophile attacks the δ^+ carbon within the *meta*-cresol isomer.

this reaction were −297 kJ mol^{-1} (*ortho*-), −299 kJ mol^{-1} (*meta*-) and −302 kJ mol^{-1} (*para*-). This channel is thus more exothermic compared to the production of $C_7H_7O^-$ because of the energetically favourable production of an H_2O molecule (reaction (11c)) compared to $OH^\bullet$ radical (reaction (11b)). Despite this, it has a considerably lower branching ratio. This may be explained by a likely increased transition energy required to produce an intermediate transition state to allow for the simultaneous removal of two H-atoms.

The other reaction pathway produced $C_6H_5O_2^-$ (reaction (11a)). Table 1 shows that this product is minor and is present at ≤2% across the isomers. This reaction exhibited ΔH values of −218 kJ mol^{-1} (*ortho*-), −220 kJ mol^{-1} (*meta*-) and −222 kJ mol^{-1} (*para*-). The low branching ratio of (11a) could be due to a barrier in the process. Note that the charge transfer reaction forming $C_7H_8O^{-\bullet}$ would be endothermic for all three isomers (according to our DFT results) by 159 kJ mol^{-1} (*ortho*- and *meta*-) and 160 kJ mol^{-1} (*para*-).

3.2.1.3 Ethylphenol. The $O^{-\bullet}$ reaction with ethylphenol formed the same two product ion species for each isomer, $C_8H_9O^-$ is the major (proton transfer); and $C_8H_7O^-$ (triple H transfer) is the minor product.

$$O^{-\bullet} + C_8H_{10}O \rightarrow C_8H_9O^- + OH^\bullet \quad (12a)$$

$$\rightarrow C_8H_7O^- + (H_2O + H^\bullet) \quad (12b)$$

The $C_8H_9O^-$ product is the predominant ion for each reaction as a lower enthalpy change of reaction is required for one H to be transferred, compared to three. The two separate pathways for the production of these product ions are shown in reactions (12a) and (12b). The change in enthalpies of reaction for reaction (12a) were −39 kJ mol^{-1} (*ortho*-), −31 kJ mol^{-1} (*meta*-) and −32 kJ mol^{-1} (*para*-); and for reaction (12b) were −78 kJ mol^{-1} (*ortho*-), −79 kJ mol^{-1} (*meta*-) and −82 kJ mol^{-1} (*para*-), noting that formation of (H_2 + $OH^\bullet$) is also exothermic but less so (by 63 kJ mol^{-1}).

Analogously to cresol, the *meta*-isomer produces the highest proportion of the proton transfer product ($C_8H_9O^-$), due to a similar charge delocalisation structure. As a result, the *meta*-ethylphenol anion transition state exhibits the lowest energy compared to the other two isomers, as the inductive effect induced by the ethyl group isn't repelled by the negative charge. This therefore produces the lowest energy transition state out of the three isomers and explains why the $C_8H_9O^-$ product has the highest branching ratio for the *meta*-ethylphenol isomer.

The rate coefficient for all three reactions is about ten times slower than k_c (Table 2), which may be due to production of neutral radicals, in both pathways. When compared to cresol, the ethylphenol reactions are slower by *ca.* 2–3 times, which may be explained by the methyl group inducing a lower +I effect compared to the ethyl group, which inherently enriches the π-system with negative charge resulting in ethylphenol being more prone at repelling the negatively charged reagent.

3.2.2 OH^- reactions

3.2.2.1 Cymene. The reactions of OH^- with the cymene isomers are observed with $C_{10}H_{13}^-$ as the major product in all three reactions by proton transfer (most likely from the isopropyl group, although it may also be taken from the methyl constituent).

$$OH^- + C_{10}H_{14} \rightarrow C_{10}H_{13}^- + H_2O \quad (13a)$$

$$\rightarrow C_8H_7O^- + C_2H_6 + H_2 \quad (13b)$$

According to our DFT calculations (for the *ortho*-isomer), channel (13a) is exothermic by 49 kJ mol^{-1} when the proton is removed from the CH_3 group, but would be endothermic for other sites. It is interesting to note that the reaction rate coefficients for proton transfer to negative ions are ten times slower than k_c, measured as 0.1 to 0.3 × 10^{-9} cm^3 s^{-1} (Table 2). The proton abstraction product (13a) was the major product in all cases (Table 1, reaction (13a)).

Table 1 shows that a 12% fraction of the minor product, $C_8H_7O^-$ is produced in the *ortho*-isomer, although its production is negligible in the *meta*- and *para*-isomers. This is reflected in the DFT results which show that the ΔH value for *ortho*-cymene is −44 kJ mol^{-1} which is more negative compared to the *meta*-isomer (−38 kJ mol^{-1}) or *para*-isomer (−38 kJ mol^{-1}). The reason for this may be down to sterical hinderance and the causation of a higher energy intermediate when the isopropyl and methyl groups are adjacent to each other.

3.2.2.2 Cresol. The reaction of OH^- with cresol proceeds again mostly by proton transfer from the cresol OH group and a minor product, $C_6H_5O^-$ is observed for the *meta*- and *para*-isomers:

$$OH^- + C_7H_8O \rightarrow C_7H_7O^- + H_2O \quad (14a)$$

$$\rightarrow C_6H_5O^- + CH_3OH \quad (14b)$$

The main products are the toloxide anion $C_7H_7O^-$ and water (reaction (14a)). This is the most dominant ion product because of the stability induced by the negative charge deposited

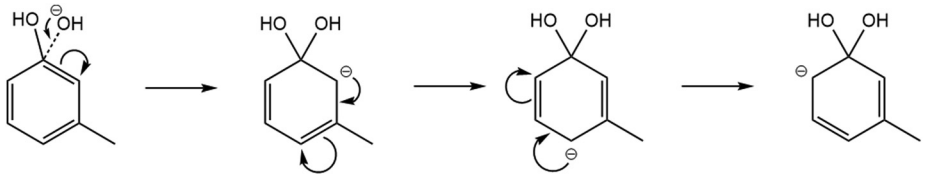

Fig. 5 Resonance stabilisation structures of the reaction anion intermediate when the OH^- nucleophile attacks the δ^+ carbon within the *meta*-cresol isomer.

(on the oxygen) which is able to delocalise throughout the π-system in the aromatic structure. The DFT calculations (for reaction (14a)) indicate relatively large ΔH values for the *ortho*-, *meta*- and *para*-cresol isomers as -182 kJ mol^{-1}, -179 kJ mol^{-1} and -176 kJ mol^{-1}, respectively.

Meta- and *para*-cresol reactions have a minor product, $C_6H_5O^-$. This is most likely from the addition of the OH^- reagent ion to the δ^+ carbon (attached to the phenolic OH group) to produce a transition state (Fig. 5). This would produce an anion intermediate which is of significantly higher energy compared to the stable major anion product, $C_7H_7O^-$. Although possible to be formed, this minor product is only seen at branching ratio percentages of 5% for *meta*-cresol and 3% for *para*-cresol. Note that in comparison with (14a) the ΔH values are less negative for (14b) (*ortho*-, *meta*- and *para*-isomers were -113 kJ mol^{-1}, -115.07 kJ mol^{-1} and -118 kJ mol^{-1}, respectively).

The mechanism shown in Fig. 5 shows the resonance structure of the possible transition states, in which the negative charge may be located in either an *ortho*- or *para*-location. Although the finishing mechanistic steps are not clear for this process, this would explain why a slightly higher branching ratio is seen for the *meta*-cresol constituent, as there is no repulsion between the +I inductive effect (by the methyl group) and the delocalised negative charge. There is however a 0% branching ratio of this minor product for *ortho*-cresol, which is most likely down to sterical hinderance causing too high energy for the transition state.

3.2.2.3 Ethylphenol. OH^- reacts with each isomer of ethylphenol by proton transfer.

$$OH^- + C_8H_{10}O \rightarrow C_8H_9O^- + H_2O \quad (15)$$

The presence of the single product ($C_8H_9O^-$) infers that the inductive effect induced by the ethyl group is low enough to still be able to stabilise the π-system within the aromatic structure to produce an intermediate which is of low enough energy for which no further fragmentation occurs, in any case.

3.2.3 $O_2^{-\bullet}$ reactions

3.2.3.1 Cymene. No reaction was observed between $O_2^{-\bullet}$ and cymene. This is not surprising as cymene is a hydrocarbon, without any electronegative atoms.

3.2.3.2 Cresol. The product ions produced on the reaction of $O_2^{-\bullet}$ with cresol indicated association[31] in parallel with proton transfer:

$$O_2^{-\bullet} + C_7H_8O + M \rightarrow C_7H_8O{\cdot}O_2^{-\bullet} + M \quad (16a)$$

$$\rightarrow C_7H_7O^- + HO_2^\bullet + M \quad (16b)$$

Channel (16b) is dominant (61% to 84%), despite the DFT calculations showing only low exothermicity ($\Delta H = -16$ kJ mol^{-1}, -12 kJ mol^{-1} and -10 kJ mol^{-1} for the *ortho*-, *meta*- and *para*-isomers, respectively) due to the production of the highly energetic $HO_2^\bullet$ radical. This means that the reaction intermediate can have a relatively long lifetime and it can be thus stabilised to form the adduct ($C_7H_8O{\cdot}O_2^{-\bullet}$). The adduct formation is exothermic by -150 kJ mol^{-1} (*ortho*-cresol), -151 kJ mol^{-1} (*meta*-cresol) and -154 kJ mol^{-1} (*para*-cresol) but this excess energy needs to be removed by a collision with the N_2 carrier gas molecules.

The slower rate coefficients (Table 2) may therefore be explained by the much more dominant pathway (reaction (16b)) possessing very low changes in enthalpy of reaction.

3.2.3.3 Ethylphenol. The $O_2^{-\bullet}$ reaction is similar to that of cresol, parallel proton transfer and three body association.

$$O_2^{-\bullet} + C_8H_{10}O + M \rightarrow C_8H_{10}O{\cdot}O_2^{-\bullet} + M \quad (17a)$$

$$\rightarrow C_8H_9O^- + HO_2^\bullet + M \quad (17b)$$

Channel 17b was found in the DFT calculations to be exothermic (by 10 kJ mol^{-1}) for the *ortho*-cresol isomer and therefore demonstrated that this reaction is energetically plausible.

3.2.4 NO_2^- and NO_3^- reactions.

Overall these ions are not very reactive. No reaction was seen between NO_2^- and cymene. Nonetheless, adduct products were detected on the reaction of NO_2^- with both cresol and ethylphenol.

$$NO_2^- + C_7H_8O + M \rightarrow C_7H_8O{\cdot}NO_2^- + M \quad (18)$$

$$NO_2^- + C_8H_{10}O + M \rightarrow C_8H_{10}O{\cdot}NO_2^- + M \quad (19)$$

NO_3^- is not a radical which explains why only an extremely slow association reaction is seen with cresol producing the adduct ion (for all isomers):

$$NO_3^- + C_7H_8O + M \rightarrow C_7H_8O{\cdot}NO_3^- + M \quad (20)$$

and why no reaction was observed for either cymene or ethylphenol. NO_2^- and NO_3^- are therefore unsuitable reagent ions to consider in the possible separate quantification of *ortho*-, *meta*- and *para*-isomeric species, of the simple aromatics presented here. *N.B.* during analysis the full scan spectra for these reactions did show some potential extra product ion peaks, although further analysis showed that these were unlikely products and were most certainly due to the presence of impurity reagent ions from the ion-source (see Section 3 of the ESI†).

4. Conclusion

In this work, we investigated positive and negative ion chemistry that could facilitate SIFT-MS analyses of some isomeric aromatic species. We have experimentally determined the reaction rate coefficients and ion product branching ratios for 72 reactions. The observed trends were substantiated by DFT calculations of the reaction thermochemistry and, to some degree, rationalised by suggested mesomeric and inductive effects and steric hindrance.

The results of this study revealed the consistency of chemistry which occurs between the SIFT-MS positive and negative reagent ions and selected aromatic species. It was found that, generally, OH^- reactions lead to the $(M–H)^-$ product; $O_2^{-\bullet}$ reactions lead to the $(M–H)^-$ product and adduct (although they are very slow); $O^{-\bullet}$ produces complicated chemistry which needs to be further investigated; and NO_2^- and NO_3^- are unreactive with these species. The differences observed for product ion branching ratios can be used to identify isomers approximately. These results, therefore, highlight the need to investigate negative ion chemistry across different chemical classes.

Conflicts of interest

There are no conflicts to declare.

Acknowledgements

The authors gratefully acknowledge financial support from the Czech Science Foundation (Grantová Agentura České Republiky, GACR; Project No. 21-25486S) and from the Praemium Academiae funding by the Czech Academy of Sciences. We would also like to thank Nicholas Demarais at Syft™ for his useful contribution to the discussion around this manuscript.

References

1 M. Phillips, K. Gleeson, J. M. B. Hughes, J. Greenberg, R. N. Cataneo, L. Baker and W. P. McVay, Volatile organic compounds in breath as markers of lung cancer: a cross-sectional study, *Lancet*, 1999, **353**, 1930–1933.

2 T. Issitt, L. Wiggins, M. Veysey, S. T. Sweeney, W. J. Brackenbury and K. Redeker, Volatile compounds in human breath: critical review and meta-analysis, *J. Breath Res.*, 2022, **16**, 024001.

3 P. Španěl and D. Smith, Progress in SIFT-MS: breath analysis and other applications, *Mass Spectrom. Rev.*, 2011, **30**, 236–267.

4 J. B. Sharmeen, F. M. Mahomoodally, G. Zengin and F. Maggi, Essential Oils as Natural Sources of Fragrance Compounds for Cosmetics and Cosmeceuticals, *Molecules*, 2021, **26**, 666.

5 K. Dryahina, S. Som, D. Smith and P. Spanel, Characterization of spoilage-related volatile organic compounds in packaged leaf salads, *Flavour Fragrance J.*, 2020, **35**, 24–33.

6 V. S. Langford, SIFT-MS: Quantifying the Volatiles You Smell. . .and the Toxics You Don't, *Chemosensors*, 2023, **11**, 111.

7 M. Ghislain, N. Costarramone, T. Pigot, M. Reyrolle, S. Lacombe and M. Le, Bechec, High frequency air monitoring by selected ion flow tube-mass spectrometry (SIFT-MS): influence of the matrix for simultaneous analysis of VOCs, CO_2, ozone and water, *Microchem. J.*, 2020, **153**, 104435.

8 A. M. Yeoman, M. Shaw, N. Carslaw, T. Murrells, N. Passant and A. C. Lewis, Simplified speciation and atmospheric volatile organic compound emission rates from non-aerosol personal care products, *Indoor Air*, 2020, **30**, 459–472.

9 M. Ghislain, M. Reyrolle, J.-M. Sotiropoulos, T. Pigot, H. Plaisance and M. Le, Bechec, Study of the Chemical Ionization of Organophosphate Esters in Air Using Selected Ion Flow Tube-Mass Spectrometry for Direct Analysis, *J. Am. Soc. Mass Spectrom.*, 2022, **33**, 865–874.

10 D. Ge, J. Zhou, Y. Chu, Y. Lu, X. Zou, L. Xia, Y. Liu, C. Huang, C. Shen, L. Zhang, H. Wang and Y. Chu, Distinguish oral-source VOCs and control their potential impact on breath biomarkers, *Anal. Bioanal. Chem.*, 2022, **414**, 2275–2284.

11 A. Gaida, O. Holz, C. Nell, S. Schuchardt, B. Lavae-Mokhtari, L. Kruse, U. Boas, J. Langejuergen, M. Allers, S. Zimmermann, C. Vogelmeier, A. R. Koczulla and J. M. Hohlfeld, A dual center study to compare breath volatile organic compounds from smokers and non-smokers with and without COPD, *J. Breath Res.*, 2016, **10**, 026006.

12 M. S. Ataabadi, S. Bahmanpour, S. Yousefinejad and S. Alaee, Blood volatile organic compounds as potential biomarkers for poly cystic ovarian syndrome (PCOS): an animal study in the PCOS rat model, *J. Steroid Biochem. Mol. Biol.*, 2023, **226**, 106215.

13 P. Španěl and D. Smith, Selected ion flow tube studies of the reactions of H_3O^+ NO^+, and O_2^+ with several aromatic and aliphatic hydrocarbons, *Int. J. Mass Spectrom.*, 1998, **181**, 1–10.

14 P. Španěl and D. Smith, Selected ion flow tube studies of the reactions of H_3O^+, NO^+, and O_2^+ with several aromatic and aliphatic monosubstituted halocarbons, *Int. J. Mass Spectrom.*, 1999, **189**, 213–223.

15 T. S. Wang, P. Španěl and D. Smith, A selected ion flow tube study of the reactions of H_3O^+, NO^+ and O_2^+ with some phenols, phenyl alcohols and cyclic carbonyl compounds in support of SIFT-MS and PTR-MS, *Int. J. Mass Spectrom.*, 2004, **239**, 139–146.

16 D. Hera, V. S. Langford, M. J. McEwan, T. I. McKellar and D. B. Milligan, Negative Reagent Ions for Real Time Detection Using SIFT-MS, *Environments*, 2017, **4**, 16.

17 M. Ghislain, N. Costarramone, J. M. Sotiropoulos, T. Pigot, R. Van Den Berg, S. Lacombe and M. Le, Bechec, Direct analysis of aldehydes and carboxylic acids in the gas phase by negative ionisation selected ion flow tube mass spectrometry: quantification and modelling of ion–molecule reactions, *Rapid Commun. Mass Spectrom.*, 2019, **33**, 1623–1634.

18 T. J. Frankcombe, OH-Initiated Oxidation of Toluene. 3. Low-Energy Routes to Cresol and Oxoheptadienal, *J. Phys. Chem. A*, 2008, **112**, 1572–1575.

19 J. Zhang, M. Choi, Y. Ji, R. Zhang, R. Zhang and Q. Ying, Assessing the Uncertainties in Ozone and SOA Predictions

due to Different Branching Ratios of the Cresol Pathway in the Toluene-OH Oxidation Mechanism, *ACS Earth Space Chem.*, 2021, **5**, 1958–1970.

20 A. M. Persico and V. Napolioni, Urinary *p*-cresol in autism spectrum disorder, *Neurotoxicol. Teratol.*, 2013, **36**, 82–90.

21 J. Faber, K. Brodzik, A. Gołda-Kopek and D. Łomankiewicz, Benzene, toluene and xylenes levels in new and used vehicles of the same model, *J. Environ. Sci.*, 2013, **25**, 2324–2330.

22 A. I. Moreno, N. Arnáiz, R. Font and A. Carratalá, Chemical characterisation of emissions from a municipal solid waste treatment plant, *Waste Manage.*, 2014, **34**, 2393–2399.

23 A. Gratien, S. N. Johnson, M. J. Ezell, M. L. Dawson, R. Bennett and B. J. Finlayson-Pitts, Surprising Formation of *p*-Cymene in the Oxidation of α-Pinene in Air by the Atmospheric Oxidants OH, O_3, and NO_3, *Environ. Sci. Technol.*, 2011, **45**, 2755–2760.

24 A. P. Pollnitz, K. H. Pardon and M. A. Sefton, Quantitative analysis of 4-ethylphenol and 4-ethylguaiacol in red wine, *J. Chromatogr. A*, 2000, **874**, 101–109.

25 R. B. Michalcikova, K. Dryahina, D. Smith and P. Španěl, Volatile compounds released by Nalophan; implications for selected ion flow tube mass spectrometry and other chemical ionisation mass spectrometry analytical methods, *Rapid Commun. Mass Spectrom.*, 2020, **34**, e8602.

26 P. Španěl, S. J. Swift, K. Dryahina and D. Smith, Relative influence of helium and nitrogen carrier gases on analyte ion branching ratios in SIFT-MS, *Int. J. Mass Spectrom.*, 2022, **476**, 116835.

27 K. Sovová, K. Dryahina and P. Španěl, Selected ion flow tube (SIFT) studies of the reactions of H_3O^+, NO^+ and $O_2^{\bullet+}$ with six volatile phytogenic esters, *Int. J. Mass Spectrom.*, 2011, **300**, 31–38.

28 T. Su and W. J. Chesnavich, Parametrization of the ion–polar molecule collision rate constant by trajectory calculations, *J. Chem. Phys.*, 1982, **76**, 5183–5185.

29 The National Institute of Standards and Technology (NIST) Chemistry WebBook, SRD 69, (**http://webbook.nist.gov/**).

30 S. J. Swift, D. Smith, K. Dryahina, M. O. Gnioua and P. Španěl, Kinetics of reactions of NH^{4+} with some biogenic organic molecules and monoterpenes in helium and nitrogen carrier gases: a potential reagent ion for selected ion flow tube mass spectrometry, *Rapid Commun. Mass Spectrom.*, 2022, **36**, e9328.

31 R. B. Michalčíková and P. Španěl, A selected ion flow tube study of the ion molecule association reactions of protonated (MH^+), nitrosonated (MNO^+) and dehydroxidated $(M–OH)^{(+)}$ carboxylic acids (M) with H_2O, *Int. J. Mass Spectrom.*, 2014, **368**, 15–22.